PHYSICAL REVIEW D **93,** 095023 (2016)

Gluino coannihilation and observability of gluinos at LHC run II

Pran Nath[*] and Andrew B. Spisak[†]

Department of Physics, Northeastern University, Boston, Massachusetts 02115-5000, USA

(Received 15 March 2016; published 26 May 2016)

The observability of a gluino at LHC run II is analyzed for the case where the gluino lies in the gluino-neutralino coannihilation region and the mass gap between the gluino and the neutralino is small. The analysis is carried out under the Higgs boson mass constraint and the constraint of dark matter relic density consistent with WMAP and Planck experiments. It is shown that in this case a gluino with mass much smaller than the current lower limit of ∼1500 GeV as given by LHC run II at 3.2 fb^{-1} of integrated luminosity would have escaped detection. The analysis is done using the signal regions used by the ATLAS Collaboration where an optimization of signal regions was carried out to determine the best regions for gluino discovery in the gluino-neutralino coannihilation region. It is shown that under the Higgs boson mass constraint and the relic density constraint, a gluino mass of ∼700 GeV would require 14 fb^{-1} of integrated luminosity for discovery and a gluino of mass ∼1250 GeV would require 3400 fb^{-1} of integrated luminosity for discovery at LHC run II. An analysis of dark matter for this case is also given. It is found that for the range of gluino masses considered, the neutralino mass lies within less than 100 GeV of the gluino mass. Thus a measurement of the gluino mass in the gluino-neutralino coannihilation region will provide a determination of the neutralino mass. In this region the neutralino is dominantly a gaugino and the spin-independent proton-neutralino cross section is small but much larger than the neutrino floor lying in the range $\sim(1\text{–}10)\times 10^{-47}$ cm^2. Thus a significant part of the parameter space of the model will lie within the reach of the next generation LUX-ZEPLIN dark matter experiment.

DOI: 10.1103/PhysRevD.93.095023

I. INTRODUCTION

The fact that sparticles have not been observed so far appears to imply that the scale of weak scale supersymmetry (SUSY) is higher than previously thought, lying in the several TeV region. This reasoning receives support from the observation that the Higgs boson [1–3] mass measurements give a mass of ∼126 GeV, [4,5] while in supersymmetry the tree-level Higgs boson mass must lie below the mass of the Z boson. Thus the extra mass must arise from loop corrections, which then requires that the SUSY scale be in the several-TeV region [6,7]. However, softly broken supersymmetry has more than one mass scale and a look at the loop correction indicates that the SUSY scale that enters is the third generation mass. Specifically, the gaugino masses are largely unconstrained and their scale could be much lower, allowing their early discovery. On the other hand, LHC data also appears to put significantly high limits, i.e. above 1.5 TeV, for the gluino mass [8].

In this work we show that in the gluino-neutralino coannihilation region, gluino masses lower than 1 TeV would have escaped detection at LHC run I and also in the analyses at LHC run II based on the accumulated integrated luminosity of 3.2 fb^{-1}. [8]. Specifically we carry out an analysis in the framework of a high-scale supergravity grand unified model [9] with radiative breaking of the electroweak symmetry (for a review see [10]). The supergravity unified models admit a large landscape for sparticle masses [11] which allows for low mass gluinos [11–14] and specifically sparticle landscapes where the gluino is the next to lowest lightest supersymmetric particle (NLSP). The largeness of the sparticle landscape arises due the fact that one may have nonuniversal supergravity models [15–17].

We investigate the sparticle spectrum in the gluino-neutralino coannihilation region under the Higgs boson mass constraints and the relic density constraint. In these models the universal scalar mass is taken to be high, lying in the several TeV region, but with low-lying gluino masses. Models we consider allow for radiative breaking of the electroweak symmetry and lie on the hyperbolic branch, [18] where large scalar masses can arise with low fine tuning. A number of works have analyzed these SUGRA models [19–25].

Here we consider the possibility that if the first and second generation GUT scale gaugino masses $m_1 = m_2$ are high while the third-generation gaugino mass m_3 is low, there can exist light gluinos with masses close to the lightest supersymmetric particle (LSP) mass that have evaded detection at the LHC so far, and may yet be discoverable at LHC run II. Coannihilation of a light gluino with mass near the LSP neutralino provides a mechanism for achieving a dark matter relic density consistent with experimental constraints from WMAP [26] and Planck [27]. The analysis shows that in the

[*]p.nath@neu.edu
[†]a.spisak@neu.edu

gluino-neutralino coannihilation region, gluino masses in the range 700–1300 Gev exist consistent with Higgs boson mass constraint and relic density constraint and would have escaped detection so far, but would be accessible at LHC run II with up to 3000 fb^{-1} of integrated luminosity. A search for signal regions for the discovery of the gluino in the gluino-neutralino coannihilation region was carried out. For each model point seven signal regions as listed by the ATLAS Collaboration [8] and displayed in Table I were analyzed. In this table, H_T is defined as the scalar sum of the transverse momentum of all jets, $M_{\rm eff}(\rm incl)$ is defined as the scalar sum of $E_T^{\rm miss}$ and the transverse momentum of all jets with $p_T > 50$ GeV, while $M_{\rm eff}(N_j)$ is the scalar sum of $E_T^{\rm miss}$ and the transverse momentum of the first N jets. Each signal region is defined by up to 12 different cuts which are on jet P_T's, $E_T^{\rm miss}$, etc., which are meant to reduce the background and enhance the signal. It is found that over the entire gluino mass region analyzed, the optimum signal regions are $2jl$ and $2jm$ (using the nomenclature of ATLAS [8]) where $2jl$ and $2jm$ are as defined in Table I.

The outline of the rest of the paper is as follows: In Sec. II we examine the parameter space of models with coannihilation of a light (<2 TeV) gluino with the LSP under the constraints of the Higgs boson mass, WMAP and Planck relic density, and LHC run I exclusions on the sparticle mass spectra. In Sec. III we carry out a signature analysis of a subset of benchmark model points for LHC run II. For these we analyze the seven signal regions of Table I and determine the leading and the subleading signal regions and the minimum integrated luminosity for LHC discovery for each of the model points analyzed. This allows us to determine the range of gluino masses which would have escaped detection thus far but would be accessible at LHC run II with up to 3000 fb^{-1} of integrated luminosity. We also compare to the latest constraints from ATLAS [8] using simplified models with 3.2 fb^{-1} of integrated luminosity for the 13 TeV data. In Sec. III C we carry out a signal region optimization. In Sec. IV we investigate the direct detection of dark matter for the benchmark points of Sec. III. Conclusions are given in Sec. V.

TABLE I. The selection criteria used for the signal regions in the nomenclature of Table II of the ATLAS analysis [8].

Requirement	Value						
	2jl	*2jm*	*2jt*	*4jt*	*5j*	*6jm*	*6jt*
$E_T^{\rm miss}$(GeV) >	200	200	200	200	200	200	200
$p_T(j_1)$(GeV) >	200	300	200	200	200	200	200
$p_T(j_2)$(GeV) >	200	50	200	100	100	100	100
$p_T(j_3)$(GeV) >	–	–	–	100	100	100	100
$p_T(j_4)$(GeV) >	–	–	–	100	100	100	100
$p_T(j_5)$(GeV) >	–	–	–	–	100	100	100
$p_T(j_6)$(GeV) >	–	–	–	–	–	100	100
$\Delta\phi(\text{jet}_{1,2,(3),E_T^{\rm miss}})_{\rm min}$ >	0.8	0.4	0.8	0.4	0.4	0.4	0.4
$\Delta\phi(\text{jet}_{i>3,E_T^{\rm miss}})_{\rm min}$ >	–	–	–	0.2	0.2	0.2	0.2
$E_T^{\rm miss}/\sqrt{H_T}(\text{GeV})^{1/2}$ >	15	15	20	–	–	–	–
$E_T^{\rm miss}/M_{\rm eff}(N_j)$ >	–	–	–	0.2	0.25	0.25	0.2
$M_{\rm eff}(\rm incl)$(GeV) >	1200	1600	2000	2200	1600	1600	2000

II. PARAMETER SPACE FOR GLUINO COANNIHILATION IN NONUNIVERSAL SUGRA

As mentioned in Sec. I, nonuniversal supergravity models allow for the possibility of nonuniversalities in the gaugino masses. In this work we consider this possibility by assuming that the scalar masses are all universal at high scale but the gaugino masses are split, i.e., gaugino masses in the $U(1)$ and $SU(2)$ sectors are equal, while the $SU(3)_C$ gaugino mass is not. Specifically we assume the following parameter space for the model:

$$m_0,\ A_0,\ m_1 = m_2 \neq m_3,\ \tan\beta,\ \text{sgn}(\mu) \qquad (1)$$

where m_0 is the universal scalar mass, $m_1 = m_2$, where m_1, m_2 are the gaugino masses for the $U(1)$ and $SU(2)$ sectors and m_3 is the $SU(3)_C$ gaugino mass, A_0 is the universal trilinear scalar coupling (all at the grand unification scale) and $\tan\beta = \langle H_2\rangle/\langle H_1\rangle$, where H_2 gives mass to the up quarks and H_1 gives mass to the down quarks and the leptons, and $\text{sgn}(\mu)$ is the sign of the Higgs mixing parameter which enters in the superpotential in the term $\mu H_1 H_2$. Using the above parameter space the sparticle spectrum is generated using SoftSusy 3.5.1 [28] while the analysis of the relic density is done using micrOMEGAs 4.1.7 [29] and SUSY Les Houches Accord-format data files are processed using PySLHA [30].

We wish to examine the region of gluino-neutralino coannihilation which requires that the gluino be the NLSP. In high scale models this can be achieved by letting m_3 lie significantly lower than the common scale $m_1 = m_2$, as shown in Table II. Thus in Table II we list several models which are chosen as illustrative examples. In generating the parameter set of Table II we have imposed the constraints that the Higgs boson mass obey $m_h = 125 \pm 2$ GeV and $\Omega h^2 = 0.11 \pm 0.013$ consistent with WMAP and Planck experiments. The ranges are chosen to take account of possible errors in theoretical computations given by codes.

Table II shows that the gluino mass lies close to the neutralino mass with their mass difference lying in the range of ∼(70–100) GeV and the gluino mass being around 1.1× the neutralino mass over essentially the entire gluino mass range. It is also to be noted that the scale of m_0 is high, lying in the several TeV region, while the light stop mass lies in the range between 2–3 TeV. The largeness of the third generation scalar masses is what provides a large loop correction to the Higgs boson to lift its tree value to the desired experimentally-observed value. The reason for the selection of the illustrative models of Table II as noted earlier is the following: As discussed in Sec. III all of the

TABLE II. A list of gluino-neutralino coannihilation models which satisfy Higgs boson mass and relic density constraints for the case when $\tan\beta = 10$ and sign(μ) is positive. All masses are in GeV. Relic density constraints were determined by taking $\pm 2.5\times$ the WMAP7 error of ± 0.0056.

Model	Gluino	Neutralino	Stop	Higgs	$\Omega_{\rm LSP}h^2$	m_0	A_0	$m_1 = m_2$	m_3
(i)	706	634	2124	123.8	0.122	5000	−7000	1400	250
(ii)	836	755	3497	124.1	0.110	7000	−8000	1650	300
(iii)	955	868	2367	125.5	0.112	6000	−9000	1900	350
(iv)	1057	975	2754	123.2	0.102	5500	−5500	2150	400
(v)	1129	1046	2910	123.5	0.101	5800	−5800	2300	430
(vi)	1201	1107	2932	126.7	0.110	7500	−11500	2400	450
(vii)	1252	1167	3459	124.1	0.101	6800	−6800	2550	480

models in Table II would have escaped detection at LHC run I but would be observable at LHC run II.

III. SIGNAL ANALYSIS FOR GLUINO-NEUTRALINO COANNIHILATION MODELS AT LHC RUN II

After applying the Higgs boson and the relic density constraints to the gluino-neutralino coannihilation region, a set of benchmark points was selected for a Monte Carlo analysis of LHC signal regions (see Table II). This analysis was performed with the MadGraph 2.2.2 [31] software system. First, the Feynman diagrams were calculated for all possible decays of the form $pp \to$ SUSY SUSY, where "SUSY" can be any MSSM particle. The analysis is configured to include both ISR and FSR jets. With the sparticle spectra of the benchmark points calculated by SoftSUSY, as well as the decay widths and branching ratios calculated by SDECAY [32,33] and HDECAY [34,35] operating within SUSY-HIT 1.5 [36], MadEvent was used to simulate 50,000 MSSM decay events for each benchmark point. Hadronization of resultant particles is handled by Pythia 6.4.28 [37], and ATLAS detector simulation and event reconstruction is performed by Delphes 3.1.2 [38]. A large set of search analyses were performed on the generated events for each benchmark point. The analyses used ROOT 5.34.21 [39] to implement search region details for the recently published 2-6 jet plus missing transverse energy signal search regions at 13 TeV [8], which look specifically for light squarks and gluons.

To allow comparison to the background, all of the signal region analyses were applied to pregenerated backgrounds published by the SNOWMASS group [40]. For each benchmark point, a calculated implied luminosity allowed direct comparison to the backgrounds. Each individual background process from the SNOWMASS background set was scaled by its own implied luminosity and combined to determine a total background count for each signal region. Figure 1 displays distributions in two key kinematic quantities, $M_{\rm eff}$ and $E_T^{\rm miss}$, for individual processes and their relative contribution to the overall background after minimal cuts for trigger simulation and a $E_T^{\rm miss} \geq 100$ GeV precut, but before any specific cuts for signal regions. Here and throughout, $M_{\rm eff}$ is specifically $M_{\rm eff}(\rm incl)$, defined as the scalar sum of $E_T^{\rm miss}$ and the p_T of all jets with $p_T(j) \geq 50$ GeV. The various background samples are grouped according to the generated final state, with a collective notation given by

$$\begin{aligned} J &= \{u, \bar{u}, d, \bar{d}, s, \bar{s}, c, \bar{c}, b, \bar{b}\}, \\ L &= \{e^+, e^-, \mu^+, \mu^-, \tau^+, \tau^-, \nu_e, \nu_\mu, \nu_\tau\}, \\ V &= \{W^+, W^-, Z, \gamma, h_0\}, \qquad T = \{t, \bar{t}\}, \\ H &= \{h_0\}. \end{aligned} \tag{2}$$

In general, events with gauge bosons and SM Higgs bosons in the final state are grouped into a single "boson" (B) category. Thus, for example, the data set "Bjj-vbf" represents production via vector boson fusion of a gauge boson or a Higgs with at least two additional light-quark jets.

A. LHC production and signal definitions

The multijet search strategy described in [8] defines seven signal regions are defined with jet multiplicities ranging from 2 to 6 jets with cuts on the inclusive effective mass $M_{\rm eff}(\rm incl)$ varying from "loose" [low $M_{\rm eff}(\rm incl)$] to "tight" [high $M_{\rm eff}(\rm incl)$]. When examining the results for the gluino coannihilation benchmark points, $2jm$ and $2jl$ were found to be the dominant and subdominant signal regions for discovery.

Using the techniques and signal regions described above, we analyzed each of the benchmark points of Table II to identify a signal region of minimum required luminosity for 5σ signal$/\sqrt{\rm background}$ discovery of this point at the LHC run II. These results can be directly compared to the results of [8] for simplified models involving gluinos and neutralinos with decoupled squarks. In that analysis it was found that for such a simplified model, using 3.2 fb^{-1} of data on the same signal regions to detect the same gluino decay channel ($\tilde{g} \to q\bar{q}\tilde{\chi}_1^0$), a gluino mass lower limit of ~1500 GeV is established for neutralino masses up to

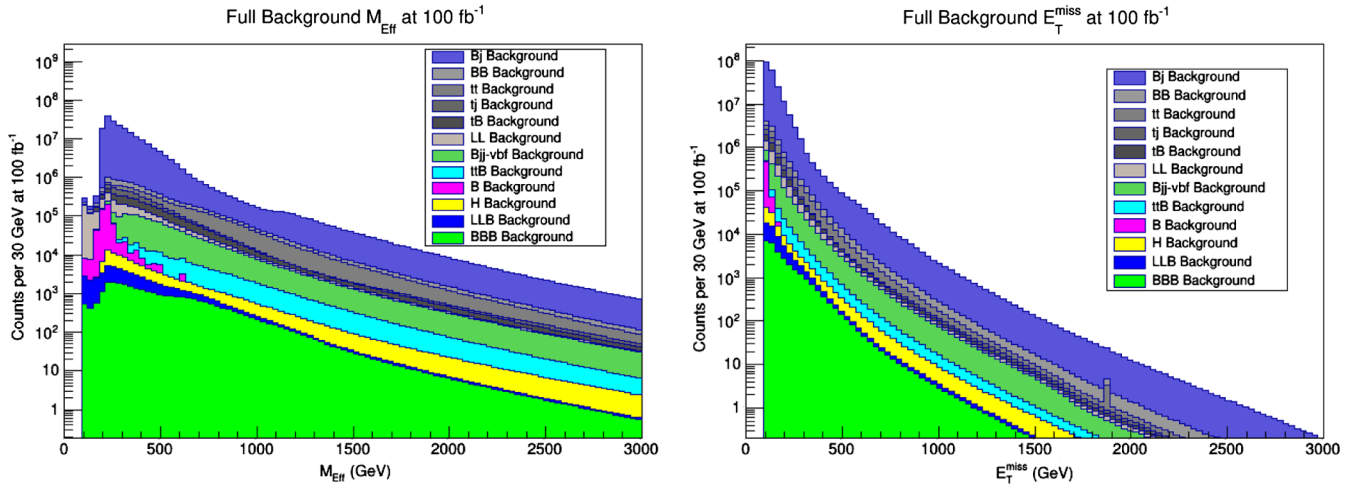

FIG. 1. A display of Standard Model SNOWMASS background after triggering cuts and a $E_T^{\rm miss} \geq 100$ GeV pre-cut. The background is broken into individual processes with the y-axis displaying the number of events per 30 GeV scaled to an integrated luminosity of 100 fb^{-1} at LHC run II. The left panel displays the distribution as a function of $M_{\rm Eff}({\rm incl})$ while the right panel displays the distribution as a function of $E_T^{\rm miss}$. Individual background processes are colored according to Eq. (3).

~800 GeV. For LSP masses above this, no exclusion is established at 3.2 fb^{-1} for any gluino masses, demonstrating that the gluino-neutralino coannihilation region remains viable for continued searching.

B. Discussion of results

In Table III we give an analysis of the SUSY production cross sections, which for the gluino-neutralino coannihilation models considered here is essentially limited to gluino pair production. The main mechanisms for gluino production are gluon fusion $gg \to \tilde{g}\tilde{g}$ and $q\bar{q} \to \tilde{g}\tilde{g}$. Because of the small mass gap between the gluino and neutralino masses needed for gluino-neutralino coannihilation, the decay of the gluino is dominated by three-body decay involving a neutralino and quarks, i.e. by the process $\tilde{g} \to q\bar{q}\tilde{\chi}_1^0$. The subleading decay is $\tilde{g} \to g\tilde{\chi}_1^0$ which is typically only a few percent with the decay mode $\tilde{g} \to q\bar{q}\tilde{\chi}_1^0$ being as much as 95% or more over most of the parameter space, as can be seen in Table III by adding the two columns on the right.

Using the signal regions defined in [8], it is found (see Table IV and Table V) that the two leading signal regions for the detection of the decay of the gluino for the gluino-neutralino coannihilation models are $2jl$ and $2jm$ over the entire range of gluino masses given in Table II. Specifically, in Table V we present a grid where the ratio signal/$\sqrt{\text{background}}$ for each of the Model (i)–(vii) for the seven signal regions is exhibited for an integrated luminosity sufficient for the discovery of the corresponding model. It is seen that for Model (i) $2jl$ is the discovery signal region while for Models (ii)–(vii), $2jm$ is the signal region for discovery. All other signal regions lie significantly below the threshold. Since for each signal region up to 12 kinematical variables with cuts are utilized, it is of interest to analyze in further detail as to the most sensitive of these kinematical quantities that allow us to discriminate the signal over the background. It is found that among the

TABLE III. SUSY production cross sections in picobarns and the gluino decay branching ratios into light quarks (u,d) and other non-top quarks (c,s,b) for gluino-neutralino coannihilation Models (i)–(vii) of Table II at LHC run II. Gluinos are pair-produced by gluon fusion via the process $gg \to \tilde{g}\tilde{g}$ as well as by $q\bar{q} \to \tilde{g}\tilde{g}$. The gluinos subsequently decay with the leading decay mode being $\tilde{g} \to q\bar{q}\tilde{\chi}_1^0$.

Model	SUSY Cross Section (pb)	BR($\tilde{g} \to q\bar{q}\tilde{\chi}_1^0$), $q \in \{u,d\}$	BR($\tilde{g} \to q\bar{q}\tilde{\chi}_1^0$), $q \in \{c,s,b\}$	BR($\tilde{g} \to g\tilde{\chi}_1^0$)
(i)	2.8	0.42	0.55	0.03
(ii)	0.95	0.43	0.56	0.02
(iii)	0.38	0.43	0.56	0.01
(iv)	0.18	0.38	0.49	0.13
(v)	0.11	0.38	0.49	0.13
(vi)	0.071	0.43	0.57	0.00
(vii)	0.051	0.39	0.51	0.10

TABLE IV. Integrated luminosity for SUSY discovery in the leading and subleading signal regions for gluino-neutralino coannihilation Models (i)–(vii) of Table II at LHC run II.

Model	Leading SR	$\mathcal{L}$ (fb^{-1})	Subleading SR	$\mathcal{L}$ (fb^{-1})
(i)	*2jl*	14	*2jm*	20
(ii)	*2jm*	66	*2jl*	71
(iii)	*2jm*	180	*2jl*	260
(iv)	*2jm*	440	*2jl*	760
(v)	*2jm*	970	*2jl*	1900
(vi)	*2jm*	2000	*2jl*	4200
(vii)	*2jm*	3400	*2jl*	7600

twelve kinematical variables, three stand out as the most sensitive for our analysis. These are $M_{\rm eff}$, $E_T^{\rm miss}$, and $E_T^{\rm miss}/\sqrt{H_T}$. We illustrate this for the cases (i), (ii), (vi), and (vii) below.

For Model (i) the sparticle mass spectrum is exhibited in Fig. 2, which shows the mass hierarchy of all the sparticle states. The sparticles lying in the mass region below 2.5 TeV have the mass hierarchy

$$m_{\tilde{\chi}_1^0} < m_{\tilde{g}} < m_{\tilde{\chi}_1^\pm} \simeq m_{\tilde{\chi}_2^0} < m_{\tilde{t}_1} < m_{\tilde{\chi}_2^\pm} \simeq m_{\tilde{\chi}_{3,4}^0}. \quad (3)$$

In the sparticle landscape this is the mass hierarchy labeled NUSP14 in the nomenclature of [12]. This hierarchy is a useful guide to what one may expect in this class of models. In the left panel of Fig. 3 we exhibit the *2jl* signal region for this model, where we plot the number of SUSY signal events (red) and the square root of the total standard model background (blue) vs. $M_{\rm Eff}$. The analysis is done for LHC run II at an integrated luminosity of 14 fb^{-1}. Similar analyses are given in the middle panel of Fig. 3 for $E_T^{\rm miss}$ and in the right panel of Fig. 3 for $E_T^{\rm miss}/\sqrt{H_T}$. Very similar analyses were carried out for Models (ii), (vi), and (vii) in Figs. 4–6. Here, however, the leading signal region is *2jm* and the analyses are done at an integrated luminosity of 66 fb^{-1} for Model (ii) in Fig. 4, at 2000 fb^{-1} for Model (vi) in Fig. 5, and at 3400 fb^{-1} for Model (vii) in Fig. 6. In each of these cases the SUSY signal meets the 5σ limit needed for discovery. A tabulation of the integrated luminosity needed for the discovery of all the models of Table II is given in Table IV.

TABLE V. A grid showing the ratio of signal divided by the square root of the background for the seven signal regions analyzed for each of the Models (i)–(vii) at the minimum $\mathcal{L}$ needed for discovery. The signal regions reaching the 5σ threshold at the minimum $\mathcal{L}$ needed for discovery are indicated in bold.

Model	$\mathcal{L}$ (fb^{-1})	*2jl*	*2jm*	*2jt*	*4jt*	*5j*	*6jm*	*6jt*
(i)	14	**5.0**	4.1	1.9	1.2	2.0	1.5	0.8
(ii)	66	4.8	**5.0**	2.5	1.8	2.0	1.1	1.0
(iii)	180	4.2	**5.0**	2.3	1.5	1.7	1.2	0.8
(iv)	440	3.8	**5.0**	2.7	1.4	1.4	0.5	0.3
(v)	970	3.6	**5.0**	3.0	1.7	1.6	1.0	1.1
(vi)	2000	3.5	**5.0**	2.8	1.6	1.4	0.5	0.5
(vii)	3400	3.3	**5.0**	3.1	1.9	1.1	0.5	0.4

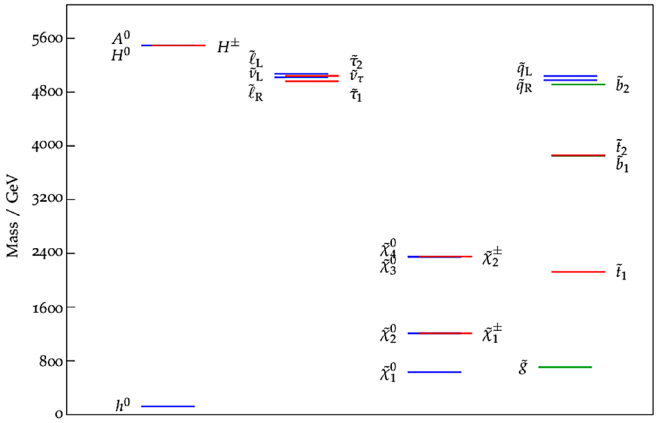

FIG. 2. An exhibition of the sparticle mass hierarchy for the gluino-neutralino coannihilation Model (i).

The analysis of Figs. 3–6 and of Table IV shows the remarkable reduction in the potential of LHC run II for the discovery of gluino if the gluino mass lies in gluino-neutralino coannihilation region. A further illustration of this result is given in Fig. 7 where the largest gluino mass discoverable as a function of the integrated luminosity at LHC run II is given if the gluino mass lies in the gluino-neutralino coannihilation region. Specifically one finds that even with ∼3000 fb^{-1} of integrated luminosity LHC run II will probe a gluino mass of ∼1200 GeV in this case. In contrast away from the gluino-neutralino coannihilation region, the discovery potential of LHC run II increases in a dramatic fashion as illustrated by the red dot in the upper left hand corner of Fig. 7, which is taken from the ATLAS analysis [8] using 3.2 fb^{-1} of integrated luminosity at LHC run II. Thus the analysis of Fig. 7 shows that if the gluino mass lies in the gluino-neutralino coannihilation region, its mass could be much smaller than the currents lower limits, where the mass gap between the gluino mass and the neutralino mass is large. In Fig. 8 we exhibit the integrated luminosity required at LHC run II for 5σ discovery of a gluino in the gluino-neutralino coannihilation region for each of the Models (i)–(vii) as a function of $\tan\beta$

C. Signal region optimization

Because the signal regions as defined in [8] are for generic simplified model light gluinos, it is advantageous to consider whether the signals can be improved upon by altering cuts to one or several of the variables in Table IV. It was found that very modest reduction (between 2 and 10 percent) in integrated luminosity required for 5σ discovery can be achieved in the $2jm$ signal region by altering the cut on the variable $E_T^{\rm miss}/\sqrt{H_T}$. To demonstrate this choice, Fig. 9 shows the results of the $2jm$ signal region in Models

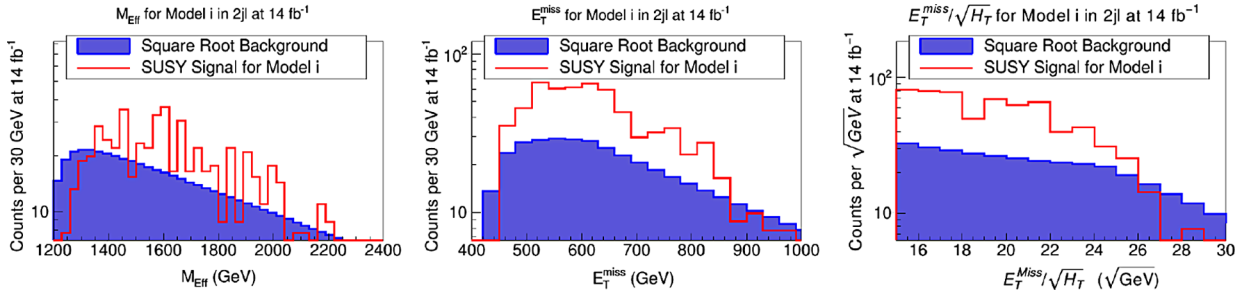

FIG. 3. Left panel: Distribution in $M_{\rm eff}$ for the $2jl$ signal region for gluino-neutralino coannihilation Model (i). Plotted is the number of counts for the SUSY signal per 30 GeV and the square root of the total SM SNOWMASS backgrounds. The analysis is done at 14 fb^{-1} of integrated luminosity at the energy scale of LHC run II, which gives a 5σ discovery in this signal region. Middle panel: The same analysis as in the left panel but for $E_T^{\rm miss}$. Right panel: The same analysis but for $E_T^{\rm miss}/\sqrt{H_T}$.

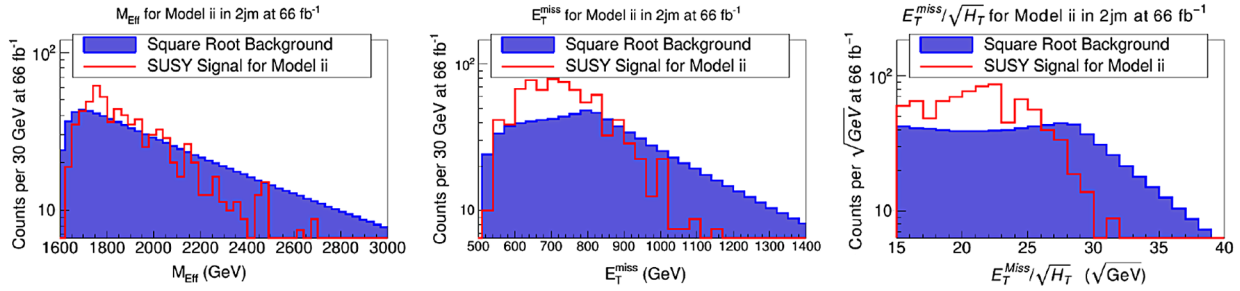

FIG. 4. Left panel: Distribution in $M_{\rm eff}$ for the $2jm$ signal region for gluino-neutralino coannihilation Model (ii). Plotted is the number of counts for the SUSY signal per 30 GeV and the square root of the total SM SNOWMASS backgrounds. The analysis is done at 66 fb^{-1} of integrated luminosity at the energy scale of LHC run II, which gives a 5σ discovery in this signal region. Middle panel: The same analysis as in the left panel but for $E_T^{\rm miss}$. Right panel: The same analysis but for $E_T^{\rm miss}/\sqrt{H_T}$.

(i), (ii), (vi), and (vii) prior to any cuts on $E_T^{\rm miss}/\sqrt{H_T}$, at the required integrated luminosity for discovery for that model.

By analyzing these figures, the original choice to require $E_T^{\rm miss}/\sqrt{H_T} > 15\sqrt{\rm GeV}$ (see Table I) is shown to be a very good choice, as this is the point where the SUSY signal (in red) overtakes the square root of the SM background (in blue). However, some improvement can be made by also requiring $E_T^{\rm miss}/\sqrt{H_T}$ to be less than a specific critical value, where the SUSY signal drops below the square root of the SM background. This occurs around the value of $25\sqrt{\rm GeV}$ for the lighter models [Model (i) and (ii)] and around $30\sqrt{\rm GeV}$ for the heavier models [Model (vi) and (vii)]. For the optimization, a value of $30\sqrt{\rm GeV}$ was chosen to optimize the fit for the heaviest gluino models, thereby extending the reach of the LHC. We call this signal region $2jm-HT$. Table VI indicates the improvement by modifying the cut on $E_T^{\rm miss}/\sqrt{H_T}$ in this way, while Fig. 10 displays the binned count data after the optimized cut. Further improvement may be possible by investigating the substructure of the jets themselves, as discussed in [41].

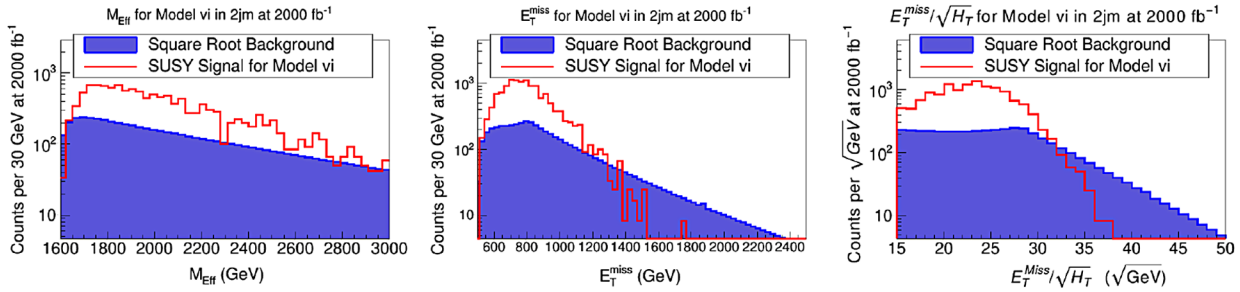

FIG. 5. Left panel: Distribution in $M_{\rm eff}$ for the $2jm$ signal region for gluino-neutralino coannihilation Model (vi). Plotted is the number of counts for the SUSY signal per 30 GeV and the square root of the total SM SNOWMASS backgrounds. The analysis is done at 2000 fb^{-1} of integrated luminosity at the energy scale of LHC run II, which gives a 5σ discovery in this signal region. Middle panel: The same analysis as in the left panel but for $E_T^{\rm miss}$. Right panel: The same analysis but for $E_T^{\rm miss}/\sqrt{H_T}$.

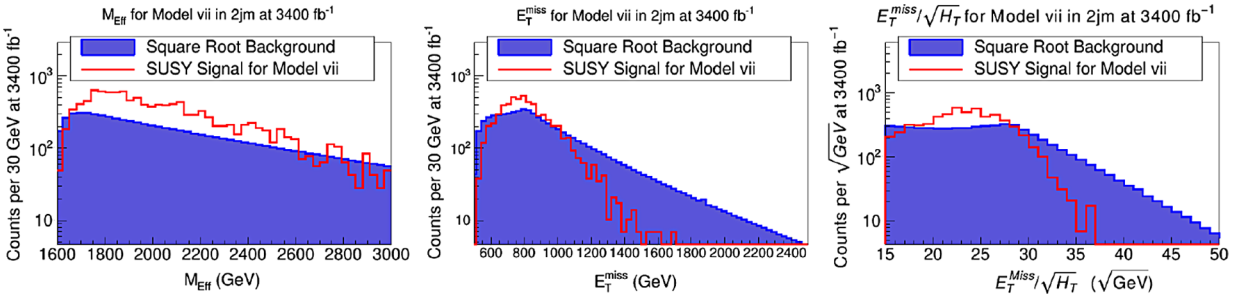

FIG. 6. Left panel: Distribution in $M_{\rm eff}$ for the $2jm$ signal region for gluino-neutralino coannihilation Model (vii). Plotted is the number of counts for the SUSY signal per 30 GeV and the square root of the total SM SNOWMASS backgrounds. The analysis is done at 3400 fb^{-1} of integrated luminosity at the energy scale of LHC run II, which gives a 5σ discovery in this signal region. Middle panel: The same analysis as in the left panel but for $E_T^{\rm miss}$. Left panel: The same analysis but for $E_T^{\rm miss}/\sqrt{H_T}$.

IV. GLUINO COANNIHILATION, LHC, AND DIRECT DETECTION OF CDM

We discuss now further details of the gluino-neutralino coannihilation model. For the case when the gluino is the NLSP the processes that enter in coannihilation are

$$\tilde{\chi}^0\tilde{\chi}^0 \to SM, \qquad \tilde{\chi}^0\tilde{g} \to SM', \qquad \tilde{g}\,\tilde{g} \to SM'', \quad (4)$$

where SM, SM', SM'' stand for standard model states. In the analysis of coannihilation the mass gap between the LSP and the NLSP plays a critical role. Thus in general for processes $\tilde{\chi}_i\tilde{\chi}_j \to SM$ the coannihilation is controlled by the ratio δ_i [42–44]

$$\delta_i = \frac{n_i^{\rm eq}}{n^{\rm eq}} = \frac{g_i(1+\Delta_i)^{3/2}e^{-\Delta_i x}}{\sum_j g_j(1+\Delta_j)^{3/2}e^{-\Delta_j x}}, \quad (5)$$

where g_i are the degrees of freedom of χ_i, $x = m_1/T$ and $\Delta_i = (m_i - m_1)/m_1$, with m_1 defined as the LSP mass and where $e^{-\Delta_i x}$ is the Boltzmann suppression factor. The relic density involves the integral

$$J_{x_f} = \int_{x_f}^{\infty} x^{-2}\langle\sigma_{\rm eff}\,v\rangle dx, \quad (6)$$

where v is the relative velocity of annihilating supersymmetric particles, $\langle\sigma_{\rm eff}\,v\rangle$ is the thermally averaged cross section times the relative velocity, and x_f is the freeze out temperature. The $\sigma_{\rm eff}$ that enters Eq. (6) has the approximate form

$$\sigma_{\rm eff} \simeq \sigma_{\tilde{g}\tilde{g}}\delta_{\tilde{\chi}^0}^2\left(\delta^2 + 2\delta\frac{\sigma_{\tilde{\chi}^0\tilde{g}}}{\sigma_{\tilde{g}\tilde{g}}} + \frac{\sigma_{\tilde{\chi}^0\tilde{\chi}^0}}{\sigma_{\tilde{g}\tilde{g}}}\right), \quad (7)$$

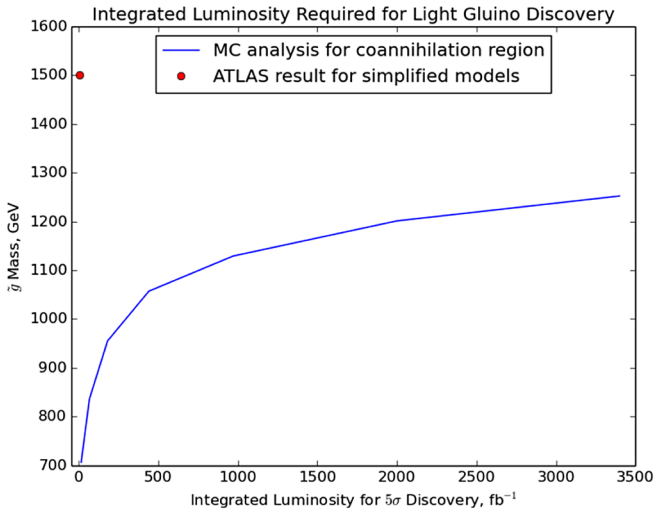

FIG. 7. Integrated luminosity required at LHC run II for 5σ discovery of gluino in the gluino-neutralino coannihilation region as a function of the gluino mass. For comparison ATLAS result from [8] using simplified models is also exhibited. One finds that the exclusion limit for the gluino mass in the coannihilation region is much lower than the ATLAS result.

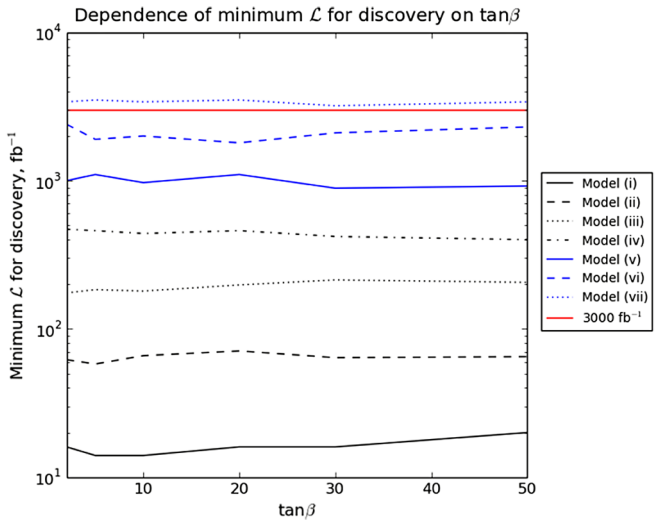

FIG. 8. Integrated luminosity required at LHC run II for 5σ discovery of a gluino in the gluino-neutralino coannihilation as a function of $\tan\beta$ for each of the Models (i)–(vii). The dependence of the integrated luminosity required for 5σ discovery is seen to have only a mild dependence on $\tan\beta$.

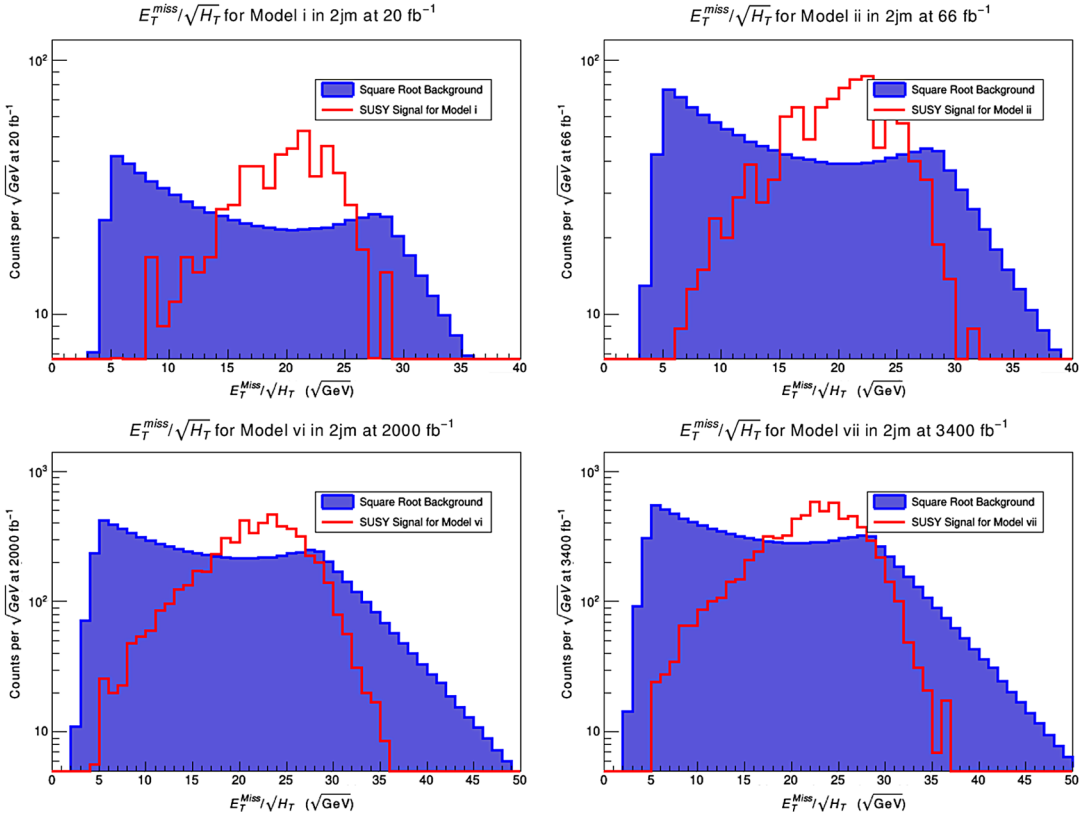

FIG. 9. Upper left panel: Distribution in $E_T^{\rm miss}/\sqrt{H_T}$ for the $2jm$ signal region for gluino-neutralino coannihilation Model (i) prior to any cuts in $E_T^{\rm miss}/\sqrt{H_T}$. The analysis is done at 20 fb^{-1} of integrated luminosity at the energy scale of LHC RUN II2, which gives a 5σ discovery in this signal region. Upper right panel: The same analysis but for Model (ii) at 66 fb^{-1} of integrated luminosity. Lower left panel: The same analysis but for Model (vi) at 2000 fb^{-1} of integrated luminosity. Lower right panel: The same analysis but for Model (vii) at 3400 fb^{-1} of integrated luminosity.

Here $\delta = \delta_{\tilde g}/\delta_{\tilde\chi^0}$ and δ_i are defined by Eq. (5). Numerical analysis shows that $\sigma_{\rm eff}$ is dominated by the processes involving the gluino such that the smaller the mass gap between the gluino and the LSP leads to more dominant gluino processes. The relic density depends critically on the mass gap and we wish to keep the relic density constant as the gluino mass increases. However, an increasing gluino mass reduces the cross section for the annihilating gluino. In order to compensate for the reduction in the gluino annihilation cross section so that $\sigma_{\rm eff}$ remains constant, the mass gap between the gluino and the LSP must decrease (see the first paper of [14] and [12]). Specifically one requires that

$$\Delta_{\tilde g\tilde\chi^0} = (m_{\tilde g}/m_{\tilde\chi^0} - 1) \tag{8}$$

must decrease as the LSP mass increases to achieve constancy of the relic density. This is what is seen in the analysis of Table II. Further, from the trend in Table II one expects that as the gluino mass gets large $m_{\tilde g}/m_{\tilde\chi^0} \to 1$ and $\Delta_{\tilde g\tilde\chi^0} \to 0$ in order to achieve relic density in the desired range. A similar phenomenon was seen in the analysis of [45].

It is pertinent to ask what the effect of nonperturbative corrections to annihilation cross section implies regarding the relic density analysis. In general, nonperturbative corrections can be significant near the threshold since here multiple gluon exchanges can occur, which produce the Sommerfeld enhancement factor. These effects may be approximated by the function $\mathcal{E}$, [13] where

$$\mathcal{E}_j = \frac{C_j\pi\alpha_s}{\beta}\left[1 - \exp\left\{-\frac{C_j\pi\alpha_s}{\beta}\right\}\right]^{-1}. \tag{9}$$

TABLE VI. Integrated luminosity for SUSY discovery in $2jm$ and $2jm$-HT, where $2jm$-HT requires that $15 < E_T^{\rm miss}/\sqrt{H_T} < 30$ in units of $\sqrt{\rm GeV}$.

Model	$\mathcal{L}$ (fb^{-1}) in $2jm$	$\mathcal{L}$ (fb^{-1}) in $2jm$-HT
(i)	20	18
(ii)	66	60
(iii)	180	170
(iv)	440	420
(v)	970	950
(vi)	2000	1980
(vii)	3400	3400

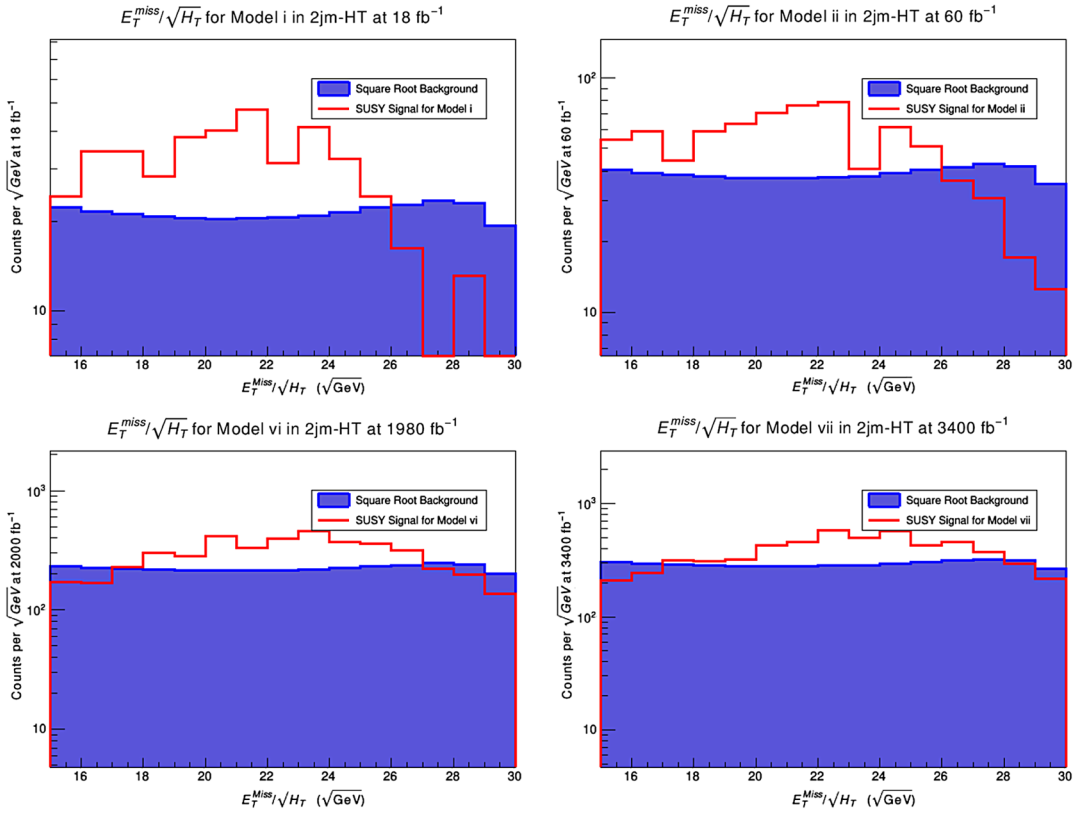

FIG. 10. Upper left panel: Distribution in $E_T^{\rm miss}/\sqrt{H_T}$ for the $2jm-HT$ signal region for gluino-neutralino coannihilation Model (i) after optimized cuts in $E_T^{\rm miss}/\sqrt{H_T}$. The analysis is done at 18 fb^{-1} of integrated luminosity at the energy scale of LHC run II, which gives a 5σ discovery in this signal region. Upper right panel: The same analysis but for Model (ii) at 60 fb^{-1} of integrated luminosity. Lower left panel: The same analysis but for Model (vi) at 1980 fb^{-1} of integrated luminosity. Lower right panel: The same analysis but for Model (vii) at 3400 fb^{-1} of integrated luminosity.

Here $C_{j=g(q)} = 1/2(3/2)$ for $\tilde{g}\,\tilde{g} \to gg$ ($\tilde{g}\,\tilde{g} \to q\bar{q}$), where $\beta = \sqrt{1-4m_{\tilde{g}}^2/s}$. In [12] an analysis was carried out for the relic density including the effect of the Sommerfeld enhancement and results compared to the one using micrOMEGAs, which uses only perturbative cross section. The analysis of [12] shows that the effect of Sommerfeld enhancement is equivalent to an upward shift of the gluino mass by 3–6 GeV without the inclusion of the Sommerfeld enhancement. Thus, based on the analysis of [12], inclusion of Sommerfeld enhancement would modify the results by only a few percent and our conclusions are not affected in any significant way.

In addition to the Sommerfeld enhancement there are also higher order QCD corrections beyond the tree-level prediction given by the code. While the inclusion of the higher order effects is beyond the scope of this work we can estimate the possible impact of such effects by enlarging the error corridor of the relic density and determine its impact on the discovery potential of LHC run II in this case for a given model point. Thus in Table VII, the $m_1 = m_2$ parameter of Model (i) is adjusted to achieve the range of Ωh^2 at the 95% confidence interval as given in [46].

The connection between LHC physics and dark matter has been discussed in the literature for some time [47] (for a review see [48]). In the context of the gluino-neutralino

TABLE VII. Effect on Model (i) of perturbing inputs to achieve Ωh^2 encompassing the 95% confidence range given in [46]. The change in the integrated luminosity needed to discover model (i) with an enlarged range of the relic density is given in the last column and the effect is less than 15% exhibiting that the analysis is robust. All mass parameters are given in GeV.

Model	$m_1 = m_2$	Gluino	Neutralino	$\Omega_{\rm LSP}h^2$	Leading SR	$\mathcal{L}$ (fb^{-1})
(i)	1400	706	634	0.122	$2jl$	14
(i-a)	1396	706	632	0.137	$2jl$	16
(i-b)	1402	706	635	0.093	$2jl$	15

TABLE VIII. Gaugino and Higgsino eigencomponents of the neutralino for gluino-neutralino coannihilation Models (i)–(vii), where $\Delta = 1 - \alpha$.

Model	$\Delta \times 10^3$	β	γ	δ
(i)	<1	−0.001	0.021	−0.008
(ii)	<1	−0.001	0.022	−0.009
(iii)	<1	−0.001	0.017	−0.006
(iv)	1	−0.003	0.042	−0.027
(v)	1	−0.003	0.042	−0.028
(vi)	<1	−0.001	0.013	−0.005
(vii)	1	−0.002	0.037	−0.024

coannihilation models the connection is even stronger. This is due to the close proximity of the neutralino mass to the gluino mass in this class of models. Thus a determination of gluino mass at the LHC would indirectly imply a determination of the neutralino mass since it lies within 10% of the gluino mass. One can thus make more definitive predictions for the direct detection of dark matter in this case. In general the neutralino has eigencomponents so that $\tilde{\chi}_1^0 = \alpha\tilde{b} + \beta\tilde{w} + \gamma\tilde{h}_1 + \delta\tilde{h}_2$, where $\tilde{b}$ is the bino, $\tilde{w}$ is the wino, and $\tilde{h}_{1,2}$ are the two Higgsinos of MSSM. The cross section for the direct detection of dark matter depends on the Higgsino content of the neutralino. The gaugino and Higgsino eigencomponents for Models (i)–(vii) are given in Table VIII. One may define the Higgsino content of the neutralino by the quantity $\sqrt{\gamma^2 + \delta^2}$. From Table VIII we see that the Higgsino content of the neutralino is typically small <0.05. A small Higgsino content indicates that the neutralino-proton cross sections will be small in the gluino-neutralino coannihilation region. This is discussed below.

In Table IX we give a computation of the spin-independent and spin-dependent proton-neutralino cross sections. For the spin-independent case one finds $\sigma^{SI}_{p\chi_1^0}$ lying in the range $(1\text{–}10) \times 10^{-47}$ cm^2. The next generation LUX-ZEPLIN dark matter experiment [49,53] is projected to reach a sensitivity of $\sim 10^{-47}$ cm^{-2} [49,53]. Thus the spin-independent proton-neutralino cross section of the gluino-neutralino coannihilation models lies largely within the sensitivity range of the next-generation LUX-ZEPLIN experiment. A graphical illustration of the spin-independent proton-neutralino cross section is given in Fig. 11. Here we are using the Models (i)–(vii) except that we allow $\tan\beta$ to vary between 2–50 and retain only those model points that satisfy the constraint $\Omega h^2 < 0.123$. One finds that all of the models lie above the neutrino floor, some by an order of magnitude or more. Thus most of the parameter points of figure 11 appear discoverable by LUX-ZEPLIN. The neutralino-proton spin dependent cross section $\sigma^{SI}_{p\chi_1^0}$ given by table IX lies in the range $(4\text{–}36) \times 10^{-45}$ cm^2. Here, LUX-ZEPLIN will have a maximum sensitivity of 10^{-42} cm^2, which is about two orders of magnitude smaller in sensitivity than what is needed to test the model in this sector.

TABLE IX. $R \times \sigma^{SI}_{p\tilde{\chi}_1^0}$ and $R \times \sigma^{SD}_{p\tilde{\chi}_1^0}$ in units of cm^2 for the gluino-neutralino coannihilation models of Table II, where $R = \rho_{\tilde{\chi}_1^0}/\rho_c$ with $\rho_{\tilde{\chi}_1^0}$ the neutralino relic density and ρ_c the critical relic density ($R \sim 1$ for the selected gluino-neutralino coannihilation model points). The Higgsino content of the neutralino in each case is also exhibited.

Model	$R \times \sigma^{SI}_{p\chi_1^0} \times 10^{47}$	$R \times \sigma^{SD}_{p\chi_1^0} \times 10^{45}$	Higgsino content
(i)	0.86	4.3	0.022
(ii)	0.92	4.9	0.024
(iii)	0.49	1.3	0.018
(iv)	7.3	35	0.050
(v)	7.2	30	0.050
(vi)	0.29	0.50	0.014
(vii)	5.5	19	0.044

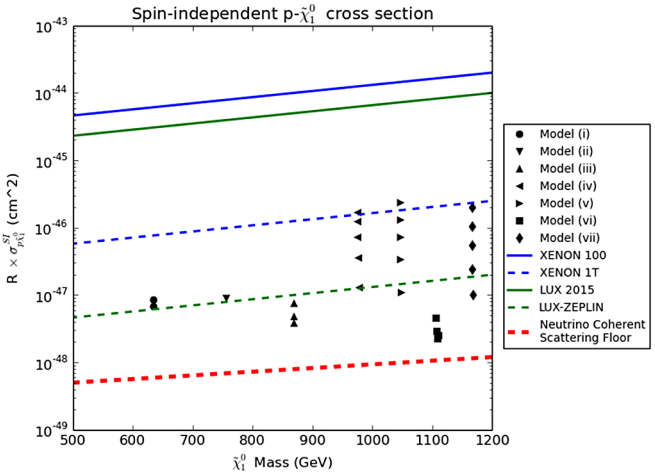

FIG. 11. $R \times \sigma^{SI}_{p,\tilde{\chi}_1^0}$ as a function of the neutralino mass where the vertical scatter points show the dependence on $\tan\beta$ in the range of $\tan\beta = 2\text{–}50$ for a given model. Only those parameter points are admitted which satisfy the constraint $\Omega h^2 < 0.123$. Also displayed are the current and projected reaches of the XENON and LUX experiments in the relevant mass range and the neutrino floor [50–53].

V. CONCLUSION

In this work it is shown that in the gluino-neutralino coannihilation region gluino masses as low as 700 GeV consistent with the Higgs boson mass constraint and the relic density constraint would have escaped detection at LHC run I and LHC run II with 3.2 fb^{-1} of integrated luminosity. Our analysis is done within the framework of high-scale supergravity models, allowing for nonuniversality in the gaugino sector. An illustrative list of models is given in Table II where the model points all satisfy the Higgs boson mass constraint and the relic density constraint consistent with WMAP and Planck. In the model space analyzed, the gluino is the NLSP, with a mass ∼1.1 times the LSP mass. The small mass gap between the

gluino and the neutralino is needed to satisfy the relic density constraint via gluino-neutralino coannihilation. Requiring that the lightest neutralino supplies all of the thermal relic abundance implies that $\Delta m = m_{\tilde{g}} - m_{\tilde{\chi}_1^0}$ lies in the range 70–100 GeV over the entire region of the parameter space analyzed in Table II. Because of the small mass gap, the gluino decay modes such as $\chi_1^{\pm} q_1 \bar{q}_2$ are suppressed and the decay occurs dominantly to $\chi_1^0 q\bar{q}$ with the subdominant decay mode being $\chi_1^0 g$. In the analysis of the Models (i)–(vii) we have used the signal regions used by the ATLAS Collaboration where an optimization of signal regions was carried out to determine the best regions for gluino discovery in the gluino-neutralino coannihilation region. It is found that among the seven signal regions analyzed the leading ones are $2jl$ and $2jm$. It is found that all the models listed in Table II are discoverable at LHC run II with up to $\sim$3400 fb^{-1} of integrated luminosity.

The implications of the gluino-neutralino coannihilation models for the discovery of dark matter was also discussed. As shown in Table IX it is found that the spin-independent neutralino-proton cross section lies in the range $(1\text{–}10) \times 10^{-47}\text{cm}^{-2}$ and this range can be explored in the next-generation experiments on dark matter, e.g. LUX-ZEPLIN [49,53]. The observed signal from the gluino-neutralino coannihilation region would be a factor of up to ten times stronger than the one from the neutrino floor [54]. Also, as shown in Table IX, the spin-dependent neutralino-proton cross section lies in the range $(0.4\text{–}4) \times 10^{-44}$ cm^2. This is about two orders of magnitude smaller than the sensitivity of LUX-ZEPLIN and thus will be more difficult to observe.

ACKNOWLEDGMENTS

This research was supported in part by the NSF Grant PHY-1314774.

[1] F. Englert and R. Brout, Broken Symmetry and the Mass of Gauge Vector Mesons, Phys. Rev. Lett. **13**, 321 (1964).
[2] P. W. Higgs, Broken Symmetries and the Masses of Gauge Bosons, Phys. Rev. Lett. **13**, 508 (1964).
[3] G. S. Guralnik, C. R. Hagen, and T. W. B. Kibble, Global Conservation Laws and Massless Particles, Phys. Rev. Lett. **13**, 585 (1964).
[4] S. Chatrchyan *et al.* (CMS Collaboration), Observation of a new boson at a mass of 125 GeV with the CMS experiment at the LHC, Phys. Lett. B **716**, 30 (2012).
[5] G. Aad *et al.* (ATLAS Collaboration), Observation of a new particle in the search for the Standard Model Higgs boson with the ATLAS detector at the LHC, Phys. Lett. B **716**, 1 (2012).
[6] S. Akula, B. Altunkaynak, D. Feldman, P. Nath, and G. Peim, Higgs boson mass predictions in SUGRA unification, recent LHC-7 results, and dark matter, Phys. Rev. D **85**, 075001 (2012).
[7] H. Baer, V. Barger, and A. Mustafayev, Implications of a 125 GeV Higgs scalar for LHC SUSY and neutralino dark matter searches, Phys. Rev. D **85**, 075010 (2012); A. Arbey, M. Battaglia, A. Djouadi, F. Mahmoudi, and J. Quevillon, Implications of a 125 GeV Higgs for supersymmetric models, Phys. Lett. B **708**, 162 (2012); P. Draper, P. Meade, M. Reece, and D. Shih, Implications of a 125 GeV Higgs for the MSSM and low-scale SUSY breaking, Phys. Rev. D **85**, 095007 (2012); M. Carena, S. Gori, N. R. Shah, and C. E. M. Wagner, A 125 GeV SM-like Higgs in the MSSM and the $\gamma\gamma$ rate, J. High Energy Phys. 03 (2012) 014; O. Buchmueller *et al.*, Higgs and supersymmetry, Eur. Phys. J. C **72**, 2020 (2012); A. Arbey, M. Battaglia, A. Djouadi, and F. Mahmoudi, The Higgs sector of the phenomenological MSSM in the light of the Higgs boson discovery, J. High Energy Phys. 09 (2012) 107; S. Akula, P. Nath, and G. Peim, Implications of the Higgs boson discovery for mSUGRA, Phys. Lett. B **717**, 188 (2012); C. Strege, G. Bertone, F. Feroz, M. Fornasa, R. Ruiz de Austri, and R. Trotta, Global fits of the cMSSM and NUHM including the LHC Higgs discovery and new XENON100 constraints, J. Cosmol. Astropart. Phys. 04 (2013) 013.
[8] The ATLAS Collaboration, Report No. ATLAS-CONF-2015-062.
[9] A. H. Chamseddine, R. Arnowitt, and P. Nath, Locally Supersymmetric Grand Unification, Phys. Rev. Lett. **49**, 970 (1982); P. Nath, R. L. Arnowitt, and A. H. Chamseddine, Gauge hierarchy in supergravity guts, Nucl. Phys. **B227**, 121 (1983); L. Hall, J. Lykken, and S. Weinberg, Supergravity as the messenger of supersymmetry breaking, Phys. Rev. D **27**, 2359 (1983); R. Arnowitt, A. H. Chamseddine, and P. Nath, The development of supergravity grand unification: Circa 1982-85, Int. J. Mod. Phys. A **27**, 1230028 (2012); **27**, 1292009 (2012).
[10] L. E. Ibanez and G. G. Ross, Supersymmetric Higgs and radiative electroweak breaking, C.R. Phys. **8**, 1013 (2007).
[11] D. Feldman, Z. Liu, and P. Nath, The Landscape of Sparticle Mass Hierarchies and Their Signature Space at the LHC, Phys. Rev. Lett. **99**, 251802 (2007); Light Higgses at the Tevatron and at the LHC and observable dark matter in SUGRA and D branes, Phys. Lett. B **662**, 190 (2008); Sparticles at the LHC, J. High Energy Phys. 04 (2008) 054; N. Chen, D. Feldman, Z. Liu, P. Nath, and G. Peim, Low mass gluino within the sparticle landscape, implications for dark matter, and early discovery prospects at LHC-7, Phys. Rev. D **83**, 035005 (2011); D. Francescone, S. Akula, B. Altunkaynak, and P. Nath, Sparticle mass hierarchies, simplified models from SUGRA unification, and benchmarks

for LHC Run-II SUSY searches, J. High Energy Phys. 01 (2015) 158.

[12] D. Feldman, Z. Liu, and P. Nath, Gluino NLSP, dark matter via gluino coannihilation, and LHC signatures, Phys. Rev. D **80**, 015007 (2009).

[13] H. Baer, K. m. Cheung, and J. F. Gunion, A heavy gluino as the lightest supersymmetric particle, Phys. Rev. D **59**, 075002 (1999); S. Raby and K. Tobe, The phenomenology of SUSY models with a gluino LSP, Nucl. Phys. **B539**, 3 (1999); H. Baer, A. Mustafayev, E. K. Park, S. Profumo, and X. Tata, Mixed Higgsino dark matter from a reduced SU(3) gaugino mass: Consequences for dark matter and collider searches, J. High Energy Phys. 04 (2006) 041.

[14] S. Profumo and C. E. Yaguna, Gluino coannihilations and heavy bino dark matter, Phys. Rev. D **69**, 115009 (2004); A statistical analysis of supersymmetric dark matter in the MSSM after WMAP, Phys. Rev. D **70**, 095004 (2004); TeV gamma-rays and the largest masses and annihilation cross sections of neutralino dark matter, Phys. Rev. D **72**, 103521 (2005); J. Ellis, F. Luo, and K. A. Olive, Gluino coannihilation revisited, J. High Energy Phys. 09 (2015) 127; J. Ellis, J. L. Evans, F. Luo, and K. A. Olive, Scenarios for gluino coannihilation, J. High Energy Phys. 02 (2016) 071; N. Bernal, A. Djouadi, and P. Slavich, The MSSM with heavy scalars, J. High Energy Phys. 07 (2007) 016; I. Gogoladze, R. Khalid, and Q. Shafi, Yukawa unification and neutralino dark matter in $SU(4)_c \times SU(2)_L \times SU(2)_R$, Phys. Rev. D **79**, 115004 (2009); A. Chatterjee, A. Choudhury, A. Datta, and B. Mukhopadhyaya, Gluino mass limits with sbottom NLSP in coannihilation scenarios, J. High Energy Phys. 01 (2015) 154; N. Nagata, H. Otono, and S. Shirai, Probing bino-gluino coannihilation at the LHC, Phys. Lett. B **748**, 24 (2015); S. Raza, Q. Shafi, and C. S. Un, NLSP gluino and NLSP stop scenarios from $b-\tau$ Yukawa unification, Phys. Rev. D **92**, 055010 (2015); B. He, T. Li, and Q. Shafi, Impact of LHC searches on NLSP top squark and gluino mass, J. High Energy Phys. 05 (2012) 148; G. Chalons and D. Sengupta, Closing in on compressed gluino-neutralino spectra at the LHC, J. High Energy Phys. 12 (2015) 129; B. Bhattacherjee, A. Choudhury, K. Ghosh, and S. Poddar, Compressed supersymmetry at 14 TeV LHC, Phys. Rev. D **89**, 037702 (2014); B. Bhattacherjee and K. Ghosh, Degenerate SUSY search at the 8 TeV LHC, arXiv:1207.6289.

[15] J. R. Ellis, K. Enqvist, D. V. Nanopoulos, and K. Tamvakis, Gaugino masses and grand unification, Phys. Lett. **155B**, 381 (1985); M. Drees, Phenomenological consequences of N = 1 supergravity theories with nonminimal kinetic energy terms for vector superfields, Phys. Lett. **158B**, 409 (1985); G. Anderson, C. H. Chen, J. F. Gunion, J. D. Lykken, T. Moroi, and Y. Yamada, Motivations for and implications of non-universal GUT-scale boundary conditions for soft SUSY-breaking parameters, eConf C960625, SUP107 (1996).

[16] P. Nath and R. Arnowitt, Non-universal soft SUSY breaking and dark matter, Phys. Rev. D **56**, 2820 (1997); J. R. Ellis, K. A. Olive, and Y. Santoso, The MSSM parameter space with non-universal Higgs masses, Phys. Lett. B **539**, 107 (2002); H. Baer, A. Mustafayev, S. Profumo, A. Belyaev, and X. Tata, Direct, indirect and collider detection of neutralino dark matter in SUSY models with non-universal Higgs masses, J. High Energy Phys. 07 (2005) 065; U. Chattopadhyay and D. Das, Higgs funnel region of supersymmetric dark matter for small tan β and renormalization group effects on pseudoscalar Higgs boson with scalar mass nonuniversality, Phys. Rev. D **79**, 035007 (2009).

[17] A. Corsetti and P. Nath, Gaugino mass nonuniversality and dark matter in SUGRA, strings and D brane models, Phys. Rev. D **64**, 125010 (2001); U. Chattopadhyay and P. Nath, $b-\tau$ unification, $g_\mu - 2$, the $\to bs+\gamma$ constraint, and nonuniversalities, Phys. Rev. D **65**, 075009 (2002); A. Birkedal-Hansen and B. D. Nelson, Relic neutralino densities and detection rates with nonuniversal gaugino masses, Phys. Rev. D **67**, 095006 (2003); U. Chattopadhyay and D. P. Roy, Higgsino dark matter in a SUGRA model with nonuniversal gaugino masses, Phys. Rev. D **68**, 033010 (2003); D. G. Cerdeno and C. Munoz, Neutralino dark matter in supergravity theories with non-universal scalar and gaugino masses, J. High Energy Phys. 10 (2004) 015; G. Belanger, F. Boudjema, A. Cottrant, A. Pukhov, and A. Semenov, WMAP constraints on SUGRA models with non-universal gaugino masses and prospects for direct detection, Nucl. Phys. **B706**, 411 (2005); H. Baer, A. Mustafayev, E. K. Park, S. Profumo, and X. Tata, Mixed Higgsino dark matter from a reduced SU(3) gaugino mass: Consequences for dark matter and collider searches, J. High Energy Phys. 04 (2006) 041; K. Choi and H. P. Nilles, The gaugino code, J. High Energy Phys. 04 (2007) 006; I. Gogoladze, R. Khalid, N. Okada, and Q. Shafi, Soft probes of SU(5) unification, Phys. Rev. D **79**, 095022 (2009); S. Bhattacharya, A. Datta, and B. Mukhopadhyaya, Non-universal gaugino and scalar masses, hadronically quiet trileptons and the Large Hadron Collider, Phys. Rev. D **78**, 115018 (2008); M. E. Gomez, S. Lola, P. Naranjo, and J. Rodriguez-Quintero, WMAP dark matter constraints on Yukawa unification with massive neutrinos, J. High Energy Phys. 04 (2009) 043; B. Altunkaynak, P. Grajek, M. Holmes, G. Kane, and B. D. Nelson, Studying gaugino mass unification at the LHC, J. High Energy Phys. 04 (2009) 114; U. Chattopadhyay, D. Das, and D. P. Roy, Mixed neutralino dark matter in nonuniversal gaugino mass models, Phys. Rev. D **79**, 095013 (2009); S. Bhattacharya and J. Chakrabortty, Gaugino mass non-universality in an SO(10) supersymmetric grand unified theory: Low-energy spectra and collider signals, Phys. Rev. D **81**, 015007 (2010); S. P. Martin, Non-universal gaugino masses from non-singlet F-terms in non-minimal unified models, Phys. Rev. D **79**, 095019 (2009).

[18] K. L. Chan, U. Chattopadhyay, and P. Nath, Naturalness, weak scale supersymmetry and the prospect for the observation of supersymmetry at the Tevatron and at the LHC, Phys. Rev. D **58**, 096004 (1998); J. L. Feng, K. T. Matchev, and T. Moroi, Multi-TeV Scalars are Natural in Minimal Supergravity, Phys. Rev. Lett. **84**, 2322 (2000); U. Chattopadhyay, A. Corsetti, and P. Nath, WMAP constraints, SUSY dark matter and implications for the direct detection of SUSY, Phys. Rev. D **68**, 035005 (2003); H. Baer, C. Balazs, A. Belyaev, T. Krupovnickas, and X. Tata, Updated reach of CERN LHC and constraints from relic density, $b \to s\gamma$ and a_μ in the mSUGRA model, J. High Energy Phys. 06 (2003) 054; M. Liu and P. Nath, Higgs boson mass, proton decay, naturalness, and constraints of the LHC and Planck

data, Phys. Rev. D **87**, 095012 (2013); S. Akula, M. Liu, P. Nath, and G. Peim, Naturalness, supersymmetry and implications for LHC and dark matter, Phys. Lett. B **709**, 192 (2012).

[19] H. Baer, V. Barger, P. Huang, D. Mickelson, A. Mustafayev, and X. Tata, Post-LHC7 fine-tuning in the minimal supergravity/CMSSM model with a 125 GeV Higgs boson, Phys. Rev. D **87**, 035017 (2013).

[20] B. Altunkaynak, M. Holmes, P. Nath, B. D. Nelson, and G. Peim, SUSY discovery potential and benchmarks for early runs at $\sqrt{s} = 7$ TeV at the LHC, Phys. Rev. D **82**, 115001 (2010).

[21] C. F. Berger, J. S. Gainer, J. L. Hewett, and T. G. Rizzo, Supersymmetry without prejudice, J. High Energy Phys. 02 (2009) 023.

[22] J. A. Conley, J. S. Gainer, J. L. Hewett, M. P. Le, and T. G. Rizzo, Supersymmetry without prejudice at the LHC, Eur. Phys. J. C **71**, 1697 (2011).

[23] L. Roszkowski, R. Ruiz de Austri, and R. Trotta, Efficient reconstruction of CMSSM parameters from LHC data: A case study, Phys. Rev. D **82**, 055003 (2010).

[24] A. Fowlie, M. Kazana, K. Kowalska, S. Munir, L. Roszkowski, E. M. Sessolo, S. Trojanowski, and Y. L. S. Tsai, The CMSSM favoring new territories: The impact of new LHC limits and a 125 GeV Higgs, Phys. Rev. D **86**, 075010 (2012).

[25] D. Kim, P. Athron, C. Balazs, B. Farmer, and E. Hutchison, Bayesian naturalness of the CMSSM and CNMSSM, Phys. Rev. D **90**, 055008 (2014).

[26] D. Larson *et al.*, Seven-Year Wilkinson Microwave Anisotropy Probe (WMAP) observations: Power spectra and WMAP-derived parameters, Astrophys. J. Suppl. Ser. **192**, 16 (2011).

[27] P. A. R. Ade *et al.* (Planck Collaboration), Planck 2015 results. XIII. Cosmological parameters, arXiv:1502.01589.

[28] B. C. Allanach, SOFTSUSY: A program for calculating supersymmetric spectra, Comput. Phys. Commun. **143**, 305 (2002).

[29] G. Belanger, F. Boudjema, A. Pukhov, and A. Semenov, micrOMEGAs: Version 1.3, Comput. Phys. Commun. **174**, 577 (2006).

[30] A. Buckley, PySLHA: A Pythonic interface to SUSY Les Houches Accord data, Eur. Phys. J. C **75**, 467 (2015).

[31] J. Alwall, R. Frederix, S. Frixione, V. Hirschi, F. Maltoni, O. Mattelaer, H.-S. Shao, T. Stelzer, P. Torrielli, and M. Zaro, The automated computation of tree-level and next-to-leading order differential cross sections, and their matching to parton shower simulations, J. High Energy Phys. 07 (2014) 079.

[32] M. Muhlleitner, SDECAY: A Fortran code for SUSY particle decays in the MSSM, Acta Phys. Pol. B **35**, 2753 (2004).

[33] M. Muhlleitner, A. Djouadi, and Y. Mambrini, SDECAY: A Fortran code for the decays of the supersymmetric particles in the MSSM, Comput. Phys. Commun. **168**, 46 (2005).

[34] A. Djouadi, J. Kalinowski, and M. Spira, HDECAY: A program for Higgs boson decays in the standard model and its supersymmetric extension, Comput. Phys. Commun. **108**, 56 (1998).

[35] M. Spira, HIGLU and HDECAY: Programs for Higgs boson production at the LHC and Higgs boson decay widths, Nucl. Instrum. Methods Phys. Res., Sect. A **389**, 357 (1997).

[36] A. Djouadi, M. M. Muhlleitner, and M. Spira, Decays of supersymmetric particles: The program SUSY-HIT (SUspect-SdecaY-Hdecay-InTerface), Acta. Phys. Pol. B **38**, 635 (2007).

[37] T. Sjostrand, S. Mrenna, and P. Z. Skands, PYTHIA 6.4 physics and manual, J. High Energy Phys. 05 (2006) 026.

[38] J. de Favereau, C. Delaere, P. Demin, A. Giammanco, V. Lemaître, A. Mertens, and M. Selvaggi (DELPHES 3 Collaboration), DELPHES 3, A modular framework for fast simulation of a generic collider experiment, J. High Energy Phys. 02 (2014) 057.

[39] Rene Brun and Fons Rademakers, ROOT—An object oriented data analysis framework, Nucl. Instrum. Methods Phys. Res., Sect. A **389**, 81 (1997). See also http://root.cern.ch/.

[40] A. Avetisyan *et al.*, Methods and Results for Standard Model Event Generation at $\sqrt{S} = 14\,TeV$, $33 TeV$ and $100\,TeV$ Proton Colliders (A Snowmass Whitepaper), arXiv:1308.1636.

[41] C. Han and M. Park, Revealing the jet substructure in a compressed spectrum, arXiv:1507.07729.

[42] K. Griest and D. Seckel, Three exceptions in the calculation of relic abundances, Phys. Rev. D **43**, 3191 (1991).

[43] P. Gondolo and G. Gelmini, Cosmic abundances of stable particles: Improved analysis, Nucl. Phys. **B360**, 145 (1991).

[44] P. Nath and R. L. Arnowitt, Predictions in SU(5) Supergravity Grand Unification with Proton Stability and Relic Density Constraints, Phys. Rev. Lett. **70**, 3696 (1993).

[45] B. Kaufman, P. Nath, B. D. Nelson, and A. B. Spisak, Light stops and observation of supersymmetry at LHC run-II, Phys. Rev. D **92**, 095021 (2015).

[46] B. Herrmann, Effect of SUSY-QCD corrections to neutralino annihilation on the cold dark matter relic density in the Higgs funnel, arXiv:0709.2232.

[47] D. Feldman, Z. Liu, P. Nath, and B. D. Nelson, Explaining PAMELA and WMAP data through coannihilations in extended SUGRA with collider implications, Phys. Rev. D **80**, 075001 (2009); M. Holmes and B. D. Nelson, Non-universal gaugino masses, CDMS, and the LHC, Phys. Rev. D **81**, 055002 (2010); D. Feldman, K. Freese, P. Nath, B. D. Nelson, and G. Peim, Predictive signatures of supersymmetry: Measuring the dark matter mass and gluino mass with early LHC data, Phys. Rev. D **84**, 015007 (2011); D. Feldman, G. Kane, R. Lu, and B. D. Nelson, Dark matter as a guide toward a light gluino at the LHC, Phys. Lett. B **687**, 363 (2010); H. Baer, V. Barger, P. Huang, and X. Tata, Natural supersymmetry: LHC, dark matter and ILC searches, J. High Energy Phys. 05 (2012) 109; L. Roszkowski, E. M. Sessolo, and A. J. Williams, What next for the CMSSM and the NUHM: Improved prospects for superpartner and dark matter detection, J. High Energy Phys. 08 (2014) 067; M. Chakraborti, U. Chattopadhyay, A. Choudhury, A. Datta, and S. Poddar, Reduced LHC constraints for Higgsino-like heavier electroweakinos, J. High Energy Phys. 11 (2015) 050; E. A. Bagnaschi, O. Buchmueller, R. Cavanaugh, M. Citron, A. De Roeck, M. J. Dolan, J. R. Ellis, H. Flecher, S. Heinemeyer, G. Isidori,

S. Malik, D. M. Santos, K. A. Olive, K. Sakurai, K. J. de Vries, and G. Weiglein, Supersymmetric dark matter after LHC run 1, Eur. Phys. J. C **75**, 500 (2015).

[48] P. Nath, B. D. Nelson *et al.*, The hunt for new physics at the Large Hadron Collider, Nucl. Phys. B, Proc. Suppl. **200–202**, 185 (2010).

[49] M. Schumann, Dark matter 2014, EPJ Web Conf. **96**, 01027 (2015).

[50] D. S. Akerib *et al.* (LUX Collaboration), Improved WIMP Scattering Limits from the LUX Experiment, Phys. Rev. Lett. **116**, 161301 (2016).

[51] E. Aprile *et al.* (XENON100 Collaboration), Dark Matter Results from 225 Live Days of XENON100 Data, Phys. Rev. Lett. **109**, 181301 (2012).

[52] F. Ruppin, J. Billard, E. Figueroa-Feliciano, and L. Strigari, Complementarity of dark matter detectors in light of the neutrino background, Phys. Rev. D **90**, 083510 (2014).

[53] P. Cushman *et al.*, Snowmass CF1 Summary: WIMP Dark Matter Direct Detection, arXiv:1310.8327.

[54] L. E. Strigari, Neutrino coherent scattering rates at direct dark matter detectors, New J. Phys. **11**, 105011 (2009).